

The Recurrent Sticky Hierarchical Dirichlet Process Hidden Markov Model

Mikołaj Słupiński

Computational Intelligence Research Group,
Institute of Computer Science, University of Wrocław,
Wrocław, Poland
{mikolaj.slupinski,piotr.lipinski}@cs.uni.wroc.pl

Piotr Lipiński

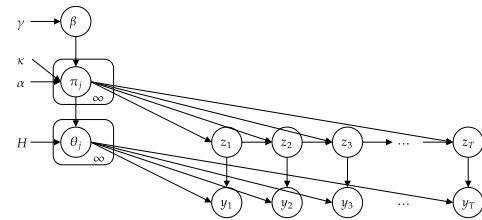
Abstract

The Hierarchical Dirichlet Process Hidden Markov Model (HDP-HMM) is a natural Bayesian nonparametric extension of the classical Hidden Markov Model for learning from (spatio-)temporal data. A sticky HDP-HMM has been proposed to strengthen the self-persistence probability in the HDP-HMM. Then, disentangled sticky HDP-HMM has been proposed to disentangle the strength of the self-persistence prior and transition prior. However, the sticky HDP-HMM assumes that the self-persistence probability is stationary, limiting its expressiveness. Here, we build on previous work on sticky HDP-HMM and disentangled sticky HDP-HMM, developing a more general model: the recurrent sticky HDP-HMM (RS-HDP-HMM). We develop a novel Gibbs sampling strategy for efficient inference in this model. We show that RS-HDP-HMM outperforms disentangled sticky HDP-HMM, sticky HDP-HMM, and HDP-HMM in both synthetic and real data segmentation.

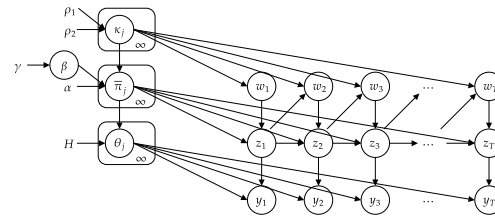
1 INTRODUCTION

Hidden Markov Models (HMMs) are more and more popular techniques for modeling not only simple time series but also more complex spatio-temporal data. They have been successfully applied to natural language processing (Suleiman et al., 2017), speech recognition (Yuan, 2012), financial time series analysis

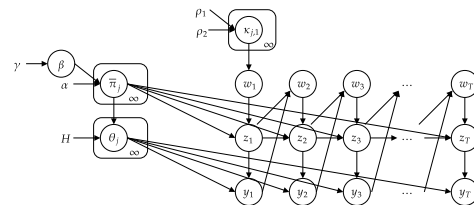
(Maruotti et al., 2019), recognition of objects movement (Arslan et al., 2019; Fielding and Ruck, 1995), etc. HMMs posit that the time series values are closely



(a) Sticky HDP-HMM



(b) Disentangled sticky HDP-HMM



(c) Recurrent sticky HDP-HMM

Figure 1: Graphical models for sticky HDP-HMM (a) and disentangled sticky HDP-HMM (b) and recurrent sticky HDP-HMM (c)

linked to hidden, time-varying states, determining the characteristics of these values. They treat the recorded time series values as observations of a certain random variable, with the current hidden state influencing its probabilistic distribution. Hidden states themselves are modeled as observations of a latent random vari-

able, with its distribution defined by the process dynamics, typically via a transition probability matrix. Learning HMM parameters from recorded data is challenging for complex datasets.

Contemporary methods like Bayesian nonparametric framework (Müller and Quintana, 2004) bypass setting the initial number of hidden states, assuming a potentially infinite number. Hierarchical Dirichlet Process Hidden Markov Model (HDP-HMM) (Teh, 2006), a key technique, uses the hierarchical Dirichlet process to model the transition matrix. Sticky HDP-HMM (SHDP-HMM) (Fox, 2009) adds a parameter to control the self-persistence probability of hidden states. Disentangled Sticky HDP-HMM (DS-HDP-HMM) (Zhou et al., 2021) further refines this by managing the self-persistence prior across hidden states.

All these methods share a common limitation: they assume stationary state-switching probabilities, which is invalid for spatio-temporal systems where movements depend on position. For instance, whether a car turns is influenced by its current location on the road. Due to their flexibility and interoperability recurrent models are widely used for neural activity analysis (Zoltowski et al., 2020; Osuna-Orozco and Santacruz, 2023; Song and Shanechi, 2023; Jiang and Rao, 2024; Bush and Ramirez, 2024) and more recently for vehicle trajectory prediction (Wei et al., 2024).

In this paper, our main contributions are: a novel approach with recurrent nonparametric modeling, extending Sticky HDP-HMM and Disentangled Sticky HDP-HMM, two efficient sampling schemes, and comparison of four Bayesian nonparametric models on a set of benchmarks.

2 BACKGROUND

2.1 Hierarchical Dirichlet Prior Hidden Markov Models

The HDP-HMM enables full Bayesian inference of HMMs. The concept is to draw a prior global transition distribution from a Dirichlet process. Then, for each hidden state, a transition distribution is taken from the shared global prior. We start by introducing some notation for the Dirichlet process (DP).

Given a base distribution H on a parameter space Θ and a positive concentration parameter γ , we construct a Dirichlet process $G \sim \text{DP}(\gamma, H)$ (sometimes also denoted by $\text{DP}(\gamma H)$) by the following stick-breaking procedure: let

$$\beta \sim \text{GEM}(\gamma), \theta_i \stackrel{iid}{\sim} H, i = 1, 2, \dots, \quad (1)$$

where $\beta \sim \text{GEM}(\gamma)$ is a random probability mass func-

tion (p.m.f.) defined on a countably infinite set as follows:

$$v_i \sim \text{Beta}(1, \gamma), \beta_i = v_i \prod_{l=1}^{i-1} (1 - v_l), i = 1, 2, \dots. \quad (2)$$

The discrete random measure $G = \sum_i \beta_i \delta_{\theta_i}$ is a sample from $\text{DP}(\gamma H)$, where δ_{θ_i} denotes the Dirac measure centered on θ_i .

The HDP-HMM uses the DP to set a prior on the rows of the HMM transition matrix in a situation where the number of latent states may be potentially infinite. HDP-HMM is defined as

$$\text{DP shared global prior: } \beta \sim \text{GEM}(\gamma), \quad (3)$$

$$\theta_j \stackrel{iid}{\sim} H, j = 1, 2, \dots, \quad (4)$$

$$\text{Transition matrix prior: } \pi_j \stackrel{iid}{\sim} \text{DP}(\alpha \beta), j = 1, 2, \dots, \quad (5)$$

$$\text{Latent states: } z_t \sim \pi_{z_{t-1}}, t = 1, \dots, T, \quad (6)$$

$$\text{Observations: } y_t \sim f(y | \theta_{z_t}), t = 1, \dots, T. \quad (7)$$

Here, β and $\{\theta_j\}_{j=1}^{\infty}$ are specified as in the DP previously described, and then each transition distribution π_j for the state j is taken as a random sample from a second DP with the base measure β and the concentration parameter α . This parameter α determines how close π_j is to the global transition distribution β . At time t , the state of a Markov chain is indicated by z_t , and the observation y_t is independently distributed given the latent state z_t and the parameters $\{\theta_j\}_{j=1}^{\infty}$, with the emission distribution $f(\cdot)$. The sticky HDP-HMM from Fox (2009) modifies the transition matrix prior by introducing a point mass distribution with a stickiness parameter κ to encourage state persistence. This is done by setting the transition matrix prior to $\pi_j \sim \text{DP}(\alpha \beta + \kappa \delta_j)$, $j = 1, 2, \dots$, where δ_j is the Dirac measure centered on j .

Zhou et al. (2021) proposed a new model - Disentangled Sticky HDP-HMM, separating the strength of self-persistence from the similarity of the transition probabilities. The authors modified the transition matrix prior as

$$\kappa_j \stackrel{iid}{\sim} \text{beta}(\rho_1, \rho_2), \quad (8)$$

$$\bar{\pi}_j \stackrel{iid}{\sim} \text{DP}(\alpha \beta), \quad (9)$$

$$\pi_j = \kappa_j \delta_j + (1 - \kappa_j) \bar{\pi}_j, j = 1, 2, \dots, \quad (10)$$

where the transition distribution π_j is a mixture distribution. A sample from π_j has the probability of

self-persistence of κ_j coming from a point mass distribution at j , and has the probability $1 - \kappa_j$ coming from $\bar{\pi}_j$, a sample from DP with a base measure β . We call this new model the disentangled sticky HDP-HMM.

2.2 Hierarchical Dirichlet Prior Hidden Markov Models

The HDP-HMM enables full Bayesian inference of HMMs. The concept is to draw a prior global transition distribution from a Dirichlet process. Then, for each hidden state, a transition distribution is taken from the shared global prior. We start by introducing some notation for the Dirichlet process (DP).

Given a base distribution H on a parameter space Θ and a positive concentration parameter γ , we construct a Dirichlet process $G \sim \text{DP}(\gamma, H)$ (sometimes also denoted by $\text{DP}(\gamma H)$) by the following stick-breaking procedure: let

$$\beta \sim \text{GEM}(\gamma), \theta_i \stackrel{iid}{\sim} H, i = 1, 2, \dots, \quad (11)$$

where $\beta \sim \text{GEM}(\gamma)$ is a random probability mass function (p.m.f.) defined on a countably infinite set as follows:

$$v_i \sim \text{Beta}(1, \gamma), \beta_i = v_i \prod_{l=1}^{i-1} (1 - v_l), i = 1, 2, \dots. \quad (12)$$

The discrete random measure $G = \sum_i \beta_i \delta_{\theta_i}$ is a sample from $\text{DP}(\gamma H)$, where δ_{θ_i} denotes the Dirac measure centered on θ_i .

The HDP-HMM uses the DP to set a prior on the rows of the HMM transition matrix in a situation where the number of latent states may be potentially infinite. HDP-HMM is defined as

$$\text{DP shared global prior: } \beta \sim \text{GEM}(\gamma), \quad (13)$$

$$\theta_j \stackrel{iid}{\sim} H, j = 1, 2, \dots, \quad (14)$$

$$\text{Transition matrix prior: } \pi_j \stackrel{iid}{\sim} \text{DP}(\alpha\beta), j = 1, 2, \dots, \quad (15)$$

$$\text{Latent states: } z_t \sim \pi_{z_{t-1}}, t = 1, \dots, T, \quad (16)$$

$$\text{Observations: } y_t \sim f(y | \theta_{z_t}), t = 1, \dots, T. \quad (17)$$

Here, β and $\{\theta_j\}_{j=1}^{\infty}$ are specified as in the DP previously described, and then each transition distribution π_j for the state j is taken as a random sample from a second DP with the base measure β and the concentration parameter α . This parameter α determines how close π_j is to the global transition distribution β . At time t , the state of a Markov chain is

denoted by z_t , and the observation y_t is independently distributed given the latent state z_t and parameters $\{\theta_j\}_{j=1}^{\infty}$, with emission distribution $f(\cdot)$. The sticky HDP-HMM from Fox (2009) modifies the transition matrix prior by introducing a point mass distribution with a stickiness parameter κ to encourage state persistence. This is done by setting the transition matrix prior to $\pi_j \sim \text{DP}(\alpha\beta + \kappa\delta_j)$, $j = 1, 2, \dots$, where δ_j is the Dirac measure centered on j .

Zhou et al. (2021) proposed a new model - Disentangled Sticky HDP-HMM, separating the strength of self-persistence from the similarity of the transition probabilities. The authors modified the transition matrix prior as

$$\kappa_j \stackrel{iid}{\sim} \text{beta}(\rho_1, \rho_2), \quad (18)$$

$$\bar{\pi}_j \stackrel{iid}{\sim} \text{DP}(\alpha\beta), \quad (19)$$

$$\pi_j = \kappa_j \delta_j + (1 - \kappa_j) \bar{\pi}_j, j = 1, 2, \dots, \quad (20)$$

where the transition distribution π_j is a mixture distribution. A sample from π_j has the probability of self-persistence of κ_j coming from a point mass distribution at j , and has the probability $1 - \kappa_j$ coming from $\bar{\pi}_j$, a sample from DP with a base measure β . We call this new model the disentangled sticky HDP-HMM.

2.3 Limitations of HDP-HMM, sticky HDP-HMM and disentangled sticky HDP-HMM

The HDP-HMM uses the concentration parameter α to modify the prior strength of the transition matrix or the similarity of the rows of the transition matrix. A high value α implies that the transition probability for each state is close to the global transition distribution β .

The sticky HDP-HMM introduces a parameter κ in comparison to the HDP-HMM. The ratio $\kappa/(\alpha + \kappa)$ determines the average probability of self-persistence or the mean of the diagonal of the transition matrix. Both the similarity of the rows of the transition matrix and the strength of prior self-persistence are regulated by $\alpha + \kappa$. The beta prior of disentangled sticky HDP-HMM (ρ_1, ρ_2) has the ability to control both the expectation of self-persistence and the variability of self-persistence. At the same time, α is free to control the variability of the transition probability around the mean transition β .

All of the models based on HDP-HMM assume that the state transition is stationary. This is especially problematic for spatio-temporal systems, where the states may be dependent on the position. To clarify, our objective is to introduce a dependency of our self-persistence parameter κ on the observation y_t . This

can be achieved by employing logistic regression.

2.4 Pólya-Gamma augmentation

One strategy that has been employed in other recurrent models for enabling efficient and quick inference (Linderman et al., 2017; Nassar et al., 2019) involves the utilization of Pólya-Gamma augmentation.

The main result of Polson et al. (2013) is that binomial probabilities can be expressed as a combination of Gaussians in terms of a Pólya-Gamma distribution. The fundamental integral identity that lies at the heart of their discovery is that, for $b > 0$,

$$\frac{(e^\psi)^a}{(1 + e^\psi)^b} = 2^{-b} e^{\lambda\psi} \int_0^\infty e^{-\omega\psi^2/2} p(\omega) d\omega. \quad (21)$$

The value of λ is calculated as the difference between a and b divided by two. The conditional distribution of ω given ψ is a Pólya-Gamma one, which makes it possible to use a Gibbs sampling approach for a variety of binomial models. This requires drawing from a Gaussian distribution for the main parameters and from a Pólya-Gamma distribution for the latent variables.

Suppose the observation of the system at time t follows

$$p(w_{t+1} | x_t) = \text{Bern}(\sigma(v_t)) = \frac{(e^{v_t})^{w_{t+1}}}{1 + e^{v_t}}, \quad (22)$$

$$v_t = R^T x_t + r,$$

where $R \in \mathbb{R}^{d_x}$, $r \in \mathbb{R}$, σ is logistic function, and Bern denotes Bernoulli distribution. Then if we introduce the PG auxiliary variables $\eta_{n,t}$, conditioning on $\eta_{1:T}$, (22) becomes

$$p(w_t | x_t, \eta_t) = e^{-\frac{1}{2}(\eta_t v_t - 2\omega_t v_t)} \\ \propto \mathcal{N}(R^T x_t + r | \omega_t/\eta_t, 1/\eta_t),$$

where $\omega_t = w_t - \frac{1}{2}$.

3 Related work

In recent years, significant work has focused on recurrent modeling. Linderman et al. (2017) introduced a method for modeling recurrence in recurrent switching linear dynamical systems (rSLDS, also known as augmented SLDS (Barber, 2005)), reducing it to a recurrent autoregressive HMM (rARHMM) via PG augmentation, similar to our approach.

Other approaches use neural networks for recurrent connections, including recurrent Hidden Semi Markov Models (Dai et al., 2016), Switching Nonlinear Dynamical Systems (Dong et al., 2020), and Recurrent Explicit Durations Switching Dynamical Systems (Ansari

et al., 2021). Recently, Geadah et al. (2023) proposed the infinite recurrent switching linear dynamic system (irSLDS). Both methods address recurrence in switching dynamics but differ substantially. Our model incorporates recurrence to influence self-persistence, unlike irSLDS, which integrates it into the state switch probability (see Eq.4).

We use Pólya-Gamma augmentation for efficient inference, whereas in irSLDS this results in intractable inference (see the Appendix of (Geadah et al., 2023)). Additionally, irSLDS uses the variational Laplace-EM algorithm for approximate posterior fitting, while we offer two MCMC sampling algorithms.

4 Recurrent sticky HDP-HMM

One of the problems of models based on HDP-HMM is that they assume stationarity of state-transition. It is especially problematic in a setting where we try to model motion.

Let us imagine that we want to model the car’s behavior. We want to make the vehicle more likely to be in the "turn" state, when it is closer to the obstacle.

To achieve position dependence we condition self-persistence on the previous observation. We can do that by performing logistic regression (given by Eq. (22)) in computing the parameter κ . To do that we use Pólya-Gamma augmentation (see Eq. (21)), which allows us for efficient Gibbs sampling. Therefore, we propose following model using notation that is in line with the conventions outlined in Section 2.2 (presented in the Figure 1(c)):

$$\text{Transition prior: } \kappa_{j,1} \stackrel{iid}{\sim} \text{beta}(\rho_1, \rho_2), \quad (23)$$

$$v_{j,t} = R_j^T y_t + r_j, \quad (24)$$

$$\kappa_{j,t+1} = \frac{(e^{v_{j,t}})}{1 + e^{v_{j,t}}}, \quad (25)$$

$$\bar{\pi}_j \stackrel{iid}{\sim} \text{DP}(\alpha\beta), \quad (26)$$

$$\pi_{j,t} = \kappa_{j,t} \delta_j + (1 - \kappa_{j,t}) \bar{\pi}_j, \quad (27)$$

$$j = 1, 2, \dots \text{ and } t = 1, \dots, T.$$

An equivalent formulation of $z_t \sim \pi_{z_{t-1}}$ in the disentangled sticky HDP-HMM is as follows:

$$\text{Latent states : } w_t \sim \text{Bern}(\kappa_{z_{t-1},t}), \\ z_t \sim w_t \delta_{z_{t-1}} + (1 - w_t) \bar{\pi}_{z_{t-1}}, \\ t = 1, \dots, T,$$

In this way, our self-persistence probability becomes position- and state-dependent. When considering motion, the likelihood of transitioning to a different state is contingent upon one’s location.

5 Inference and Learning

Algorithm 1 Direct assignment sampler for RS-HDP-HMM

- 1: Sequentially sample $\{z_t, w_t, w_{t+1}\}$ for $t = 1, \dots, T$.
 - 2: Sample $\{\kappa_{j,1}\}$ for $j = 1, \dots, K + 1$, and compute $\{\kappa_{j,t+1}\}$ for $t = 1, \dots, T - 1, j = 1, \dots, K + 1$. K is defined as number of unique states in $\{z_t\}_{t=1}^T$.
 - 3: Sequentially sample auxiliary variables $\{\eta_{j,t}\}$ for $t = 1, \dots, T - 1, j = 1, \dots, K + 1$.
 - 4: Sample β . (Same as HDP-HMM).
 - 5: Sample hyperparameter $\alpha, \gamma, \rho_1, \rho_2, R$.
-

5.1 Direct Assignment Sampler

The direct assignment sampler marginalizes transition distributions π_j and parameters θ_j and sequentially samples z_t given all the other states $z_{\setminus t}$, observations $\{y_t\}_{t=1}^T$, and the global transition distribution β .

Our direct assignment sampler is based on the direct assignment sampler for DS-HDP-HMM, which means that instead of only sampling z_t (as in the sampler for HDP-HMM), we sample $\{z_t, w_t, w_{t+1}\}$ in blocks. We sample α, β, γ only using z_t that switch to other states by $\bar{\pi}_{z_{t-1}}$ ($w_t = 0$), and sample $\{\kappa_{j,t}\}_{j=1}^{K+1}, \rho_1, \rho_2$ only using z_t that stick to state z_{t-1} ($w_t = 1$). The main difference between the samplers presented by Fox et al. (2011); Zhou et al. (2021) comes from the fact that κ_j is now a vector and we have to additionally sample the auxiliary variables.

Algorithm 1 presents direct assignment sampler steps. For Step 1, we compute the probability of each possible posterior case of $p(z_t, w_t, w_{t+1} \mid z_{\setminus t}, w_{\setminus \{t,t+1\}}, \{y_t\}_{t=1}^T, \alpha, \beta, \{\kappa_{j,1:T}\}_{j=1}^{K+1})$ in sequence and sample the corresponding categorical distribution for $\{z_t, w_t, w_{t+1}\}$, where all states except z_t are denoted by $z_{\setminus t}$, and all w_t except for w_t and w_{t+1} are represented by $w_{\setminus \{t,t+1\}}$. If $z_t = K + 1$, that is, a new state appears, we increment K , sample the regression parameters R_{K+1} for the new state from the prior state, and update β using stick breaking. This requires $\mathcal{O}(TK)$ operations.

For Step 2, given w_{t+1} whose corresponding z_t is j , we sample $\kappa_{j,1}$ using beta-binomial conjugacy and compute $\kappa_{j,t}$ using Equation (22), performing the $\mathcal{O}(TK)$ steps.

Step 3 involves sampling $T(K + 1)$ auxiliary variables, requiring $\mathcal{O}(TK)$ steps.

Step 4 involves introducing auxiliary variables $\{m_{jk}\}_{j,k=1}^K$ and sampling β using Dirichlet categorical conjugacy, which requires $\mathcal{O}(K)$ draws.

Step 5 computes the empirical transition matrix $\{n_{jk}\}_{j,k=1}^K$, where n_{jk} is the number of transitions from state j to k with $w_t = 0$ in $\{z_t\}_{t=1}^T$, and introduces additional auxiliary variables. Then the posteriors of α and γ are conjugated with Gamma, given the auxiliary variables. We approximate the posterior of ρ_1, ρ_2 by finite grids. This last step has a computational complexity of $\mathcal{O}(K)$. The total complexity per iteration is $\mathcal{O}(TK)$.

As mentioned in the study by Fox et al. (2011), when the entire latent sequence $\{z_t, w_t\}_{t=1}^T$ is sampled jointly, it significantly improves the mixing rate. This is particularly crucial for models with dynamics, such as ARHMM and SLDS, where the correlated observations can further slow down the mixing rate of the direct assignment sampler. For this reason, we did not utilize this sampler in our experiments. However, we have included its description for the sake of comprehensiveness in this study.

5.2 Weak-Limit Sampler

The weak-limit sampler for the sticky HDP-HMM takes advantage of the fact that the Dirichlet process is a discrete measure to produce a finite approximation of the HDP prior. This approximation converges to the HDP prior when the number of components, L , goes to infinity (Ishwaran and Zarepour, 2000, 2002). The standard HMM forward-backward procedure can be used to sample latent variables $\{z_t\}_{t=1}^T$ with the help of this approximation, which increases the mixing rate of the Gibbs sampler. Our weak-limit Gibbs sampler is based on the sampler for DS-HDP-HMM, so it samples pairs $\{z_t, w_t\}_{t=1}^T$.

Algorithm 2 Weak-limit sampler for RS-HDP-HMM

- 1: Jointly sample $\{z_t, w_t\}_{t=1}^T$.
 - 2: Sample $\{\kappa_{j,1}\}$ for $j = 1, \dots, L$, and compute $\{\kappa_{j,t+1}\}$ for $t = 1, \dots, T - 1, j = 1, \dots, L$.
 - 3: Sequentially sample auxiliary variables $\{\eta_{j,t}\}$ for $t = 1, \dots, T - 1, j = 1, \dots, L$.
 - 4: Sample $\{\beta_j\}_{j=1}^L, \{\bar{\pi}_j\}_{j=1}^L$. (Same as HDP-HMM).
 - 5: Sample $\{\theta_j\}_{j=1}^L$.
 - 6: Sample hyperparameter $\alpha, \gamma, \rho_1, \rho_2, R$.
-

Algorithm 2 presents weak-limit sampler steps. In Step 1, we use the forward-backward procedure to jointly sample the two-dimensional latent variables

$\{z_t, w_t\}_{t=1}^T$.

Step 2 is the same as in the direct assignment sampler.

Step 3 is the same as in the direct assignment sampler.

For Step 4, we sample β and $\bar{\pi}$ based on Dirichlet-categorical conjugacy, given the auxiliary variables $\{m_{jk}\}_{j,k=1}^L$, the empirical transition matrix $\{n_{jk}\}_{j,k=1}^L$, and the approximate prior.

Step 5 involves placing a conjugate prior in θ_j and using conjugacy to sample the posterior. Step 5 is the same as in the direct assignment sampler. The complexity of each step is $\mathcal{O}(TL^2)$, $\mathcal{O}(L)$, $\mathcal{O}(L)$, $\mathcal{O}(L)$, and $\mathcal{O}(L)$, respectively, with a total complexity of $\mathcal{O}(TL^2)$.

The beam sampling technique (Van Gael et al., 2008; Dewar et al., 2012; Słupiński and Lipiński, 2024) is a useful method for sampling the approximation parameter L , eliminating the need to pre-set it while still allowing the transition matrix to be instantiated and the state sequence to be block sampled. This is especially beneficial when the number of states is too large to be accurately estimated beforehand. In this paper, we will not examine beam sampling.

6 Experiments

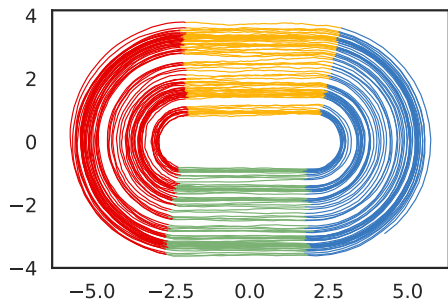


Figure 2: Trajectory of *NASCAR*[®] used to test the models.

To evaluate our motion segmentation model’s effectiveness, we compared it against HDP-HMM, sticky HDP-HMM, and disentangled sticky HDP-HMM on three benchmarks. The HDP-HMM benchmarks used the implementation from Zhou et al. (2021).¹

We employed the Matrix Normal inverse-Wishart (MNIW(M, V, S, n)) prior for autoregressive emission in all experiments, detailed in Fox et al. (2011). Specifically, $M_0 = \mathbf{0}$ and $V_0 = I$ were selected to center the prior’s mass around stable matrices. The inverse-Wishart component had $n_0 = m + 2$ degrees

of freedom, with the scale matrix S_0 set to $0.4\bar{\Sigma}$, where $\bar{\Sigma}$ is defined as $\frac{1}{T-1} \sum (x_t - \bar{x})(x_t - \bar{x})^T$ and $x_t = y_{t+1} - y_t$.

All models used a Gamma (1, 0.01) prior for concentration parameters α , and $\alpha + \kappa$ for sticky HDP-HMM. To avoid numerical instability in sampling β by preventing extreme γ values, a Gamma (2,1) prior was used for γ .

Self-persistence parameters employed non-informative priors: a uniform distribution in $[0, 1]$ for $\phi = \frac{\rho_1}{\rho_1 + \rho_2}$, and for DS-HDP-HMM, a uniform distribution in $[0, 2]$ for $\eta = (\rho_1 + \rho_2)^{-1/3}$. The support of ϕ and η was partitioned into a 100×100 grid for simulated data. The prior for (R, r) was $\mathcal{N}(0, 0.0001 \cdot I)$.

Log-likelihood was our primary metric to compare models, with higher values indicating a better fit. This metric provides a straightforward probabilistic comparison, as employed in Zhou et al. (2021); Fox (2009). We also used accuracy and F1 scores for assessing segmentation quality.

For quantitative evaluation, we used the dancing bee and *NASCAR*[®] benchmarks, widely used in Bayesian motion segmentation studies (Oh et al., 2008; Fox et al., 2011; Linderman et al., 2017; Nassar et al., 2019). For qualitative evaluation, we chose the mouse behavior dataset, a key dataset in self-supervised segmentation research (Zhou et al., 2021; Batty et al., 2019; Costacurta et al., 2022). All of the sampler runs were performed on Intel Xeon Platinum 8268 using two cores.

6.1 *NASCAR*[®]

We begin with a straightforward illustration where the dynamics take the form of oval shapes, resembling a stock car on a *NASCAR*[®] track. The dynamics is determined by four distinct states, $z_t \in \{1, \dots, 4\}$, which regulate a continuous latent state in two dimensions, $y_t \in \mathbb{R}^2$.

For this experiment, we performed ten runs with different random seeds. The results are averaged.

We can distinguish four states here, which are presented in Figure 2. To make the states more distinguishable, the car uses four different velocities (which can be observed in Figure 5, as the segments differ significantly in length).

It is evident that the state of the system is influenced by its position. As the car completes each lap, it spends a greater amount of time in the “straight-on” states. This poses a challenge for models that have a constant transition matrix, as the probability of self-persistence follows a Geometric distribution.

¹<https://github.com/zhd96/ds-hdp-hmm>

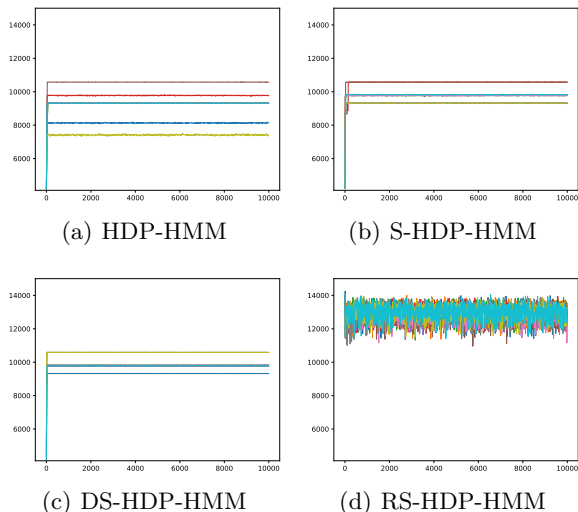


Figure 3: Log-likelihood during models’ fitting on *NASCAR*[®] dataset. Our model obtains the highest likelihood scores. It presents a diverse range of likelihood scores within a single run. Additionally, we observe that the other models often converge to local optima. Furthermore, the RS-HDP-HMM model exhibits a considerably shorter burn-in time.

Table 1: Results of *NASCAR*[®] data segmentation.

	Weighted F1	Accuracy
HDP-HMM	0.86	0.82
S-HDP-HMM	0.91	0.88
DS-HDP-HMM	0.94	0.95
RS-HDP-HMM	0.97	0.97

The segmentation outcomes are demonstrated in Table 1. It is evident that our model exhibits superior performance. Figure 5 illustrates that the remaining models occasionally struggle to differentiate the fourth state.

The results obtained from Figures 4 and 3 demonstrate that our model achieves the highest likelihood scores and produces the most coherent outcomes. Nevertheless, it is important to mention that it also exhibits the largest variance in likelihood in a single run.

6.2 Dancing Bee

We employed the publicly available dancing bees dataset (Oh et al., 2008), which is renowned for its intricate characteristics and has previously been studied in the field of time series segmentation.

The dataset consists of the trajectories followed by six honey bees while performing the waggle dance, including their 2D coordinates and heading angle at each

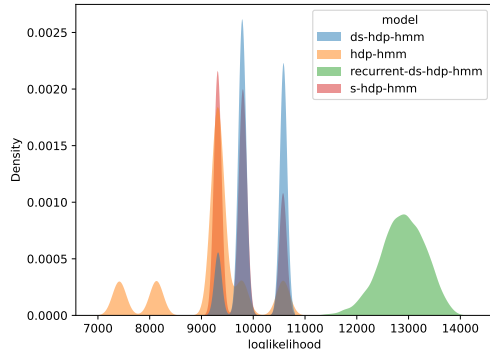


Figure 4: Distribution of *NASCAR*[®] log-likelihoods taken after 200 burn-in iterations. Our model attains the highest likelihood scores and generates the most coherent results. However, it is worth noting that it also demonstrates the greatest variability in likelihood within a single execution.

time step. The bees demonstrate three types of motion: waggle, turn right, and turn left.

Table 2: Results of dancing bee data segmentation.

	Weighted F1	Accuracy
HDP-HMM	0.73	0.77
S-HDP-HMM	0.85	0.87
DS-HDP-HMM	0.83	0.84
RS-HDP-HMM	0.85	0.87

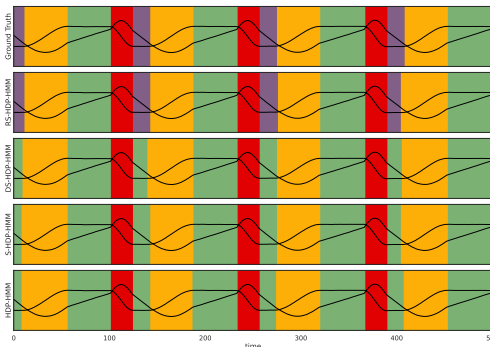


Figure 5: Sample results of *NASCAR*[®] segmentation. The color represents an assigned segment. Methods other than RS-HDP-HMM often fail to differentiate two ”straight” states.

Honey bees communicate the whereabouts of food sources by performing a series of dances within the hive. These dances consist of waggle, turn right, and turn left movements. The waggle dance of a bee consists of it walking in a straight line while shaking its body from side to side quickly. The turning dances are simply the bee rotating clock-

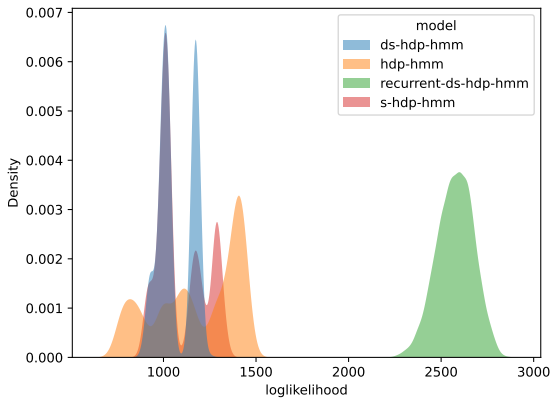


Figure 6: Distribution of models’ log-likelihoods taken after 2000 burn-in iterations on dancing bee dataset. Our model achieves the highest likelihood scores, demonstrating a clear unimodal distribution of likelihood scores. Furthermore, we observe that the other models often become trapped in local optima.

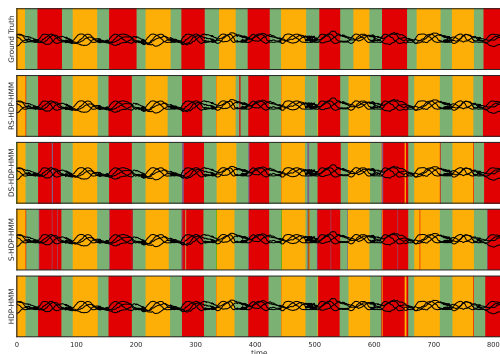


Figure 7: Results of dancing bee dataset. The color represents an assigned segment. The segmentation obtained from our model is the smoothest.

wise or counterclockwise. The data consist of $\mathbf{y}_t = [\cos(\theta_t), \sin(\theta_t), x_t, y_t]^T$, where (x_t, y_t) denotes the 2D coordinates of the body of the bee and θ_t its head angle.

For this experiment, we performed ten runs with different random seeds. The results are averaged.

We can see in Table 2 that our model performed on a par with S-HDP-HMM in terms of accuracy and weighted F1. However, in Figure 7 we can observe that the segmentation obtained from our model is the smoothest.

In the same graph, it is evident that the values observed during the "waggle" phase are significantly smaller in magnitude compared to those obtained during turning. We hypothesize that this characteristic enables our model to achieve a more seamless segmen-

tation.

Like the previous experiment, the findings shown in Figures 6 and 8 demonstrate that our model achieves the highest likelihood scores and produces the most coherent outcomes. Additionally, it exhibits the greatest range of likelihood scores in a single execution.

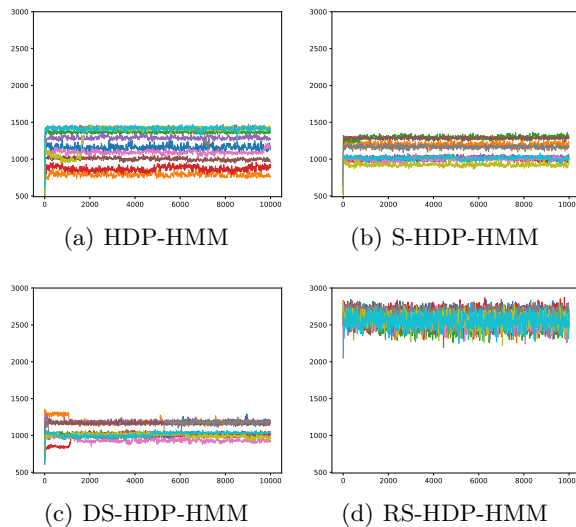


Figure 8: Log-likelihood during models’ fitting on honey bee movements. Our model achieves the highest likelihood scores and generates the most coherent results. However, it demonstrates the widest range of likelihood scores within a single execution. We can also see that it has significantly smaller burn-in time.

6.3 Mouse Behavior

Our model was also tested on a publicly accessible mouse behavior dataset. In the described experiment, the mouse was immobilized by fixing its head position during a visual decision-making task. During this task, neural activities in the dorsal cortex were monitored through wide-field calcium imaging. The behavioral video data comprised grayscale frames with a resolution of 128x128 pixels. This video was recorded from two different angles using two cameras, one for the side view and another for the bottom view. To manage the high-dimensional nature of the video data, we adopted dimension reduction techniques previously established. These involved 9-dimensional continuous variables derived through a convolutional autoencoder (Batty et al., 2019).

In real-world scenarios, ARHMM models often suffer from a problem called over-segmentation. This refers to the situation where behaviors that seem similar to a human expert are divided into separate clusters. According to the hypothesis proposed by Costacurta

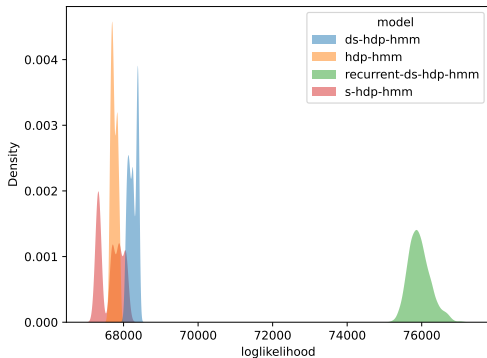


Figure 9: Distribution of log-likelihoods on mouse behavior dataset taken after 9000 burn-in iterations. In line with previous findings, our model attains the highest likelihood scores, indicating a distinct unimodal distribution of likelihood scores with the greatest variation within each run. Additionally, we note that the other models do not converge to a shared optimal solution.

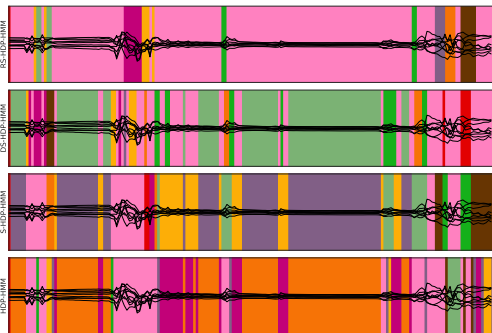


Figure 10: Results of mouse behavior dataset. The color represents an assigned segment. One issue frequently encountered in ARHMM models is known as over-segmentation. However, RS-HDP-HMM segmentation, despite utilizing a similar number of states as DS-HDP-HMM, offers a smoother and more stable alternative.

et al. (2022), over-segmentation occurs because the ARHMM model confuses discrete factors of behavioral variability, such as the expression of different behavioral syllables, with continuous factors of variability that cannot be adequately represented using linear autoregressive dynamics with Gaussian noise.

We performed five independent MCMC runs for all model types. On average, RS-HDP-HMM converged to 33 states, DS-HDP-HMM to 34, S-HDP-HMM to 21 and HDP-HMM to 23 states. On average there were 6143 state switches for RS-HDP-HMM, 7713 for DS-HDP-HMM, 6412 for S-HDP-HMM and 7801 for HDP-HMM.

Despite using nearly as many states as DS-HDP-HMM, RS-HDP-HMM segmentation remains much smoother and more stable. A sample segmentation is presented in Figure 10. For example, in the pink state, our model demonstrates a greater tolerance for minor noise. This is because it considers not only the direction of position change but also the actual position. Therefore, even if the direction changes, as long as the position change is small enough, there will be no transition to a different state.

7 Conclusions and Future Work

The paper presents a new modeling technique that combines latent states with position- and state-dependent self-persistence probability. This technique is particularly suitable for motion data, where the likelihood of transitioning to a different state depends on the subject’s location.

A central contribution of this paper is introducing dependence of stickiness factor on the previous observations.

The RS-HDP-HMM addresses a significant limitation in conventional HMMs: their inability to effectively model non-Markovian temporal dependencies. Many real-world processes exhibit behaviors where the current state depends not just on the immediate past state (as in hidden Markov models), but on a more complex history of previous states. Similar level of contribution was introduced by RSLDS or iRSLDS bringing similar dependence to SLDS.

The recurrent model consistently demonstrates better performance metrics, showcasing its strength in capturing data nuances, and the obtained states are more robust to small noise, as it is shown by mouse behavior dataset.

Similarly to Zhou et al. (2021) who modified the algorithms introduced by Fox (2009), we introduce two sampling schemes for our model.

Acknowledgements

Calculations have been carried out using resources provided by Wrocław Centre for Networking and Supercomputing (<http://wcss.pl>), grant No. 405.

This work was supported by the Polish National Science Centre (NCN) under grant OPUS-18 no. 2019/35/B/ST6/04379.

References

Ansari, A. F., Benidis, K., Kurle, R., Turkmen, A. C., Soh, H., Smola, A. J., Wang, B., and Januschowski,

- T. (2021). Deep Explicit Duration Switching Models for Time Series. In *Advances in Neural Information Processing Systems*, volume 34, pages 29949–29961. Curran Associates, Inc.
- Arslan, M., Cruz, C., and Ginhac, D. (2019). Semantic trajectory insights for worker safety in dynamic environments. *Autom. Constr.*, 106:102854.
- Barber, D. (2005). Expectation Correction for an augmented class of Switching Linear Gaussian Models.
- Batty, E., Whiteway, M., Saxena, S., Biderman, D., Abe, T., Musall, S., Gillis, W., Markowitz, J., Churchland, A., Cunningham, J. P., Datta, S. R., Linderman, S., and Paninski, L. (2019). BehaveNet: nonlinear embedding and Bayesian neural decoding of behavioral videos. In *Advances in Neural Information Processing Systems*, volume 32. Curran Associates, Inc.
- Bush, N. E. and Ramirez, J.-M. (2024). Latent neural population dynamics underlying breathing, opioid-induced respiratory depression and gasping. *Nat Neurosci*, 27(2):259–271.
- Costacurta, J. C., Duncker, L., Sheffer, B., Gillis, W., Weinreb, C., Markowitz, J. E., Datta, S. R., Williams, A. H., and Linderman, S. W. (2022). Distinguishing discrete and continuous behavioral variability using warped autoregressive HMMs.
- Dai, H., Dai, B., Zhang, Y., Li, S., and Song, L. (2016). Recurrent Hidden Semi-Markov Model.
- Dewar, M., Wiggins, C., and Wood, F. (2012). Inference in Hidden Markov Models with Explicit State Duration Distributions. *IEEE Signal Processing Letters*, 19(4):235–238.
- Dong, Z., Seybold, B., Murphy, K., and Bui, H. (2020). Collapsed Amortized Variational Inference for Switching Nonlinear Dynamical Systems. In *Proceedings of the 37th International Conference on Machine Learning*, pages 2638–2647. PMLR.
- Escobar, M. D. and West, M. (1995). Bayesian Density Estimation and Inference Using Mixtures. *Journal of the American Statistical Association*, 90(430):577–588.
- Fielding, K. and Ruck, D. (1995). Spatiotemporal Pattern-Recognition Using Hidden Markov-Models. *IEEE Trans. Aerosp. Electron. Syst.*, 31(4):1292–1300.
- Fox, E., Sudderth, E. B., Jordan, M. I., and Willsky, A. S. (2011). Bayesian Nonparametric Inference of Switching Dynamic Linear Models. *IEEE Transactions on Signal Processing*, 59(4):1569–1585.
- Fox, E. B. (2009). *Bayesian nonparametric learning of complex dynamical phenomena*. Thesis, Massachusetts Institute of Technology.
- Geadah, V., Laboratory, I. B., and Pillow, J. W. (2023). Parsing neural dynamics with infinite recurrent switching linear dynamical systems.
- Ishwaran, H. and Zarepour, M. (2000). Markov Chain Monte Carlo in Approximate Dirichlet and Beta Two-Parameter Process Hierarchical Models. *Biometrika*, 87(2):371–390.
- Ishwaran, H. and Zarepour, M. (2002). Dirichlet Prior Sieves in Finite Normal Mixtures. *Statistica Sinica*, 12(3):941–963.
- Jiang, L. P. and Rao, R. P. N. (2024). Dynamic predictive coding: A model of hierarchical sequence learning and prediction in the neocortex. *PLoS Comput. Biol.*, 20(2):e1011801.
- Linderman, S., Johnson, M., Miller, A., Adams, R., Blei, D., and Paninski, L. (2017). Bayesian Learning and Inference in Recurrent Switching Linear Dynamical Systems. In *Proceedings of the 20th International Conference on Artificial Intelligence and Statistics*, pages 914–922. PMLR.
- Maruotti, A., Punzo, A., and Bagnato, L. (2019). Hidden Markov and Semi-Markov Models with Multivariate Leptokurtic-Normal Components for Robust Modeling of Daily Returns Series. *J. Financ. Econom.*, 17(1):91–117.
- Müller, P. and Quintana, F. A. (2004). Nonparametric Bayesian Data Analysis. *Statistical Science*, 19(1):95–110.
- Nassar, J., Linderman, S. W., Bugallo, M. F., and Park, I. M. (2019). Tree-Structured Recurrent Switching Linear Dynamical Systems for Multi-Scale Modeling. In *7th International Conference on Learning Representations, ICLR 2019, New Orleans, LA, USA, May 6-9, 2019*. OpenReview.net.
- Oh, S., Rehg, J., Balch, T., and Dellaert, F. (2008). Learning and Inferring Motion Patterns using Parametric Segmental Switching Linear Dynamic Systems. *International Journal of Computer Vision*, 77.
- Osuna-Orozco, R. and Santacruz, S. R. (2023). Identification of Switching Linear Dynamics in Distributed Neural Populations. In *11th International IEEE EMBS Conference on Neural Engineering (IEEE/EMBS NER)*, New York. IEEE.
- Polson, N. G., Scott, J. G., and Windle, J. (2013). Bayesian Inference for Logistic Models Using Pólya–Gamma Latent Variables. *Journal of the American Statistical Association*, 108(504):1339–1349.
- Song, C. Y. and Shanechi, M. M. (2023). Unsupervised learning of stationary and switching dynamical system models from Poisson observations. *J. Neural Eng.*, 20(6):066029.

- Suleiman, D., Awajan, A., and Al Etaiwi, W. (2017). The Use of Hidden Markov Model in Natural ARABIC Language Processing: a survey. In *8th International Conference on Emerging Ubiquitous Systems and Pervasive Networks (EUSPN) / 7th International Conference on Current and Future Trends of Information and Communication Technologies in Healthcare (ICTH)*, volume 113, pages 240–247, Amsterdam. Elsevier Science Bv.
- Słupiński, M. and Lipiński, P. (2024). Improving SLDS Performance Using Explicit Duration Variables with Infinite Support. In *Neural Information Processing*, Communications in Computer and Information Science, pages 112–123, Singapore. Springer Nature.
- Teh, Y. W. (2006). A Hierarchical Bayesian Language Model Based On Pitman-Yor Processes. In *Proceedings of the 21st International Conference on Computational Linguistics and 44th Annual Meeting of the Association for Computational Linguistics*, pages 985–992, Sydney, Australia. Association for Computational Linguistics.
- Van Gael, J., Saatchi, Y., Teh, Y. W., and Ghahramani, Z. (2008). Beam sampling for the infinite hidden Markov model. In *Proceedings of the 25th international conference on Machine learning, ICML '08*, pages 1088–1095, New York, NY, USA. Association for Computing Machinery.
- Wei, R., Lee, J., Wakayama, S., Tschantz, A., Heins, C., Buckley, C., Carenbauer, J., Thiruvengada, H., Albarracín, M., Prado, M. d., Horling, P., Winzell, P., and Rajagopal, R. (2024). Navigation under uncertainty: Trajectory prediction and occlusion reasoning with switching dynamical systems.
- Yuan, L.-c. (2012). Improved hidden Markov model for speech recognition and POS tagging. *J. Cent. South Univ.*, 19(2):511–516.
- Zhou, D., Gao, Y., and Paninski, L. (2021). Disentangled Sticky Hierarchical Dirichlet Process Hidden Markov Model. volume 12457, pages 612–627, Cham. Springer International Publishing.
- Zoltowski, D., Pillow, J., and Linderman, S. (2020). A general recurrent state space framework for modeling neural dynamics during decision-making. In *Proceedings of the 37th International Conference on Machine Learning*, pages 11680–11691. PMLR.

A Sampling Scheme

Step 1 is analogous to Fox et al. (2011) and Zhou et al. (2021). We describe it here for completeness.

Step 1: Sequentially Sample z_t, w_t, w_{t+1} : The posterior distribution of z_t, w_t , and w_{t+1} is expressed as follows:

$$\begin{aligned} & p(z_t = k, w_t, w_{t+1} \mid z_{\setminus t}, w_{\setminus \{t, t+1\}}, y_{1:T}, \alpha, \beta, \{\kappa_{j,1:T}\}_{j=1}^{K+1}) \\ & \propto p(z_t = k, w_t, w_{t+1} \mid z_{\setminus t}, w_{\setminus \{t, t+1\}}, \alpha, \beta, \{\kappa_{j,1:T}\}_{j=1}^{K+1}) \cdot p(y_t \mid y_{\setminus t}, z_t = k, z_{\setminus t}). \end{aligned} \quad (28)$$

where all observations except y_t are denoted by $y_{\setminus t}$, and all w_t except for w_t and w_{t+1} are represented by $w_{\setminus \{t, t+1\}}$.

The predictive observation likelihood $p(y_t \mid y_{\setminus t}, z_t = k, z_{\setminus t})$ can be quickly calculated if we use a conjugate prior on the parameter in the observation likelihood.

$$\begin{aligned} & p(z_t = k, w_t, w_{t+1} \mid z_{\setminus t}, w_{\setminus \{t, t+1\}}, \alpha, \beta, \{\kappa_{j,1:T}\}_{j=1}^{K+1}) \\ & \propto p(z_t = k, w_t, w_{t+1}, z_{t+1} \mid z_{\setminus \{t, t+1\}}, w_{\setminus \{t, t+1\}}, \alpha, \beta, \{\kappa_{j,1:T}\}_{j=1}^{K+1}) \\ & \propto \int_{\bar{\pi}} p(w_t \mid \kappa_{z_{t-1}, t}) p(z_t \mid w_t, \bar{\pi}_{z_{t-1}}) p(w_{t+1} \mid \kappa_{z_t, t+1}) p(z_{t+1} \mid w_{t+1}, \bar{\pi}_{z_t}) \\ & \quad \prod_i \left(\prod_{\tau \mid z_{\tau-1}=i, w_\tau=0, \tau \neq t, t+1} p(\bar{\pi}_i \mid \alpha, \beta) p(z_\tau \mid \bar{\pi}_i) \right) d\bar{\pi} \\ & \propto \int_{\bar{\pi}} p(w_t \mid \kappa_{z_{t-1}, t}) p(z_t \mid w_t, \bar{\pi}_{z_{t-1}}) p(w_{t+1} \mid \kappa_{z_t, t+1}) p(z_{t+1} \mid w_{t+1}, \bar{\pi}_{z_t}) \\ & \quad \prod_i p(\bar{\pi}_i \mid \{z_{\tau-1} = i, w_\tau = 0, \tau \neq t, t+1\}, \alpha, \beta) d\bar{\pi}. \end{aligned} \quad (29)$$

Let $z_{t-1} = j, z_{t+1} = l$, then Equation (29) simplifies to

$$\begin{cases}
 \kappa_{j,t} \kappa_{j,t+1}, & \text{if } w_t = w_{t+1} = 1, k = j = l \\
 (1 - \kappa_{j,t}) \kappa_{l,t+1} \int_{\bar{\pi}_j} p(z_t = l | w_t, \bar{\pi}_j) p(\bar{\pi}_j | \{\tau | z_{\tau-1} = j, w_\tau = 0, \tau \neq t\}, \alpha, \beta) d\bar{\pi}_j, & \text{if } w_t = 0, w_{t+1} = 1, k = l \\
 (1 - \kappa_{j,t}) \kappa_{j,t} \int_{\bar{\pi}_j} p(z_{t+1} = l | w_{t+1}, \bar{\pi}_j) p(\bar{\pi}_j | \{\tau | z_{\tau-1} = j, w_\tau = 0, \tau \neq t+1\}, \alpha, \beta) d\bar{\pi}_j, & \text{if } w_t = 1, w_{t+1} = 0, k = j \\
 (1 - \kappa_{j,t}) (1 - \kappa_{k,t+1}) \int_{\bar{\pi}_j} p(z_t = k | w_t, \bar{\pi}_j) p(\bar{\pi}_j | \{\tau | z_{\tau-1} = j, w_\tau = 0, \tau \neq t\}, \alpha, \beta) d\bar{\pi}_j, & \\
 \int_{\bar{\pi}_k} p(z_{t+1} = l | w_{t+1}, \bar{\pi}_k) p(\bar{\pi}_k | \{\tau | z_{\tau-1} = k, w_\tau = 0, \tau \neq t+1\}, \alpha, \beta) d\bar{\pi}_k, & \text{if } w_t = 0, w_{t+1} = 0, k \neq j \\
 (1 - \kappa_{j,t}) (1 - \kappa_{k,t+1}) & \\
 \int_{\bar{\pi}_j} p(z_t = j | w_t, \bar{\pi}_j) p(z_{t+1} = l | w_{t+1}, \bar{\pi}_j) p(\bar{\pi}_j | \{\tau | z_{\tau-1} = j, w_\tau = 0, \tau \neq t, t+1\}, \alpha, \beta) d\bar{\pi}_j, & \text{if } w_t = 0, w_{t+1} = 0, k = j \\
 0, & \text{otherwise}
 \end{cases}$$

The result is the following equations:

$$\begin{aligned}
 \int_{\bar{\pi}_j} p(z_t = k | w_t, \bar{\pi}_j) p(\bar{\pi}_j | \{\tau | z_{\tau-1} = j, w_\tau = 0, \tau \neq t\}, \alpha, \beta) d\bar{\pi}_j &= \frac{\alpha \beta_k + n_{jk}^{-t}}{\alpha + n_j^{-t}}, \\
 \int_{\bar{\pi}_k} p(z_{t+1} = l | w_{t+1}, \bar{\pi}_k) p(\bar{\pi}_k | \{\tau | z_{\tau-1} = k, w_\tau = 0, \tau \neq t+1\}, \alpha, \beta) d\bar{\pi}_k &= \frac{\alpha \beta_l + n_{kl}^{-t}}{\alpha + n_k^{-t}}, \\
 \int_{\bar{\pi}_j} p(z_t = j | w_t, \bar{\pi}_j) p(z_{t+1} = l | w_{t+1}, \bar{\pi}_j) p(\bar{\pi}_j | \{\tau | z_{\tau-1} = j, w_\tau = 0, \tau \neq t, t+1\}, \alpha, \beta) d\bar{\pi}_j \\
 &= \frac{(\alpha \beta_j + n_{jj}^{-t}) (\alpha \beta_l + n_{jl}^{-t} + \delta(j, l))}{(\alpha + n_j^{-t}) (\alpha + n_j^{-t} + 1)}, \\
 \int_{\bar{\pi}_j} p(z_t = k | w_t, \bar{\pi}_j) p(\bar{\pi}_j | \{\tau | z_{\tau-1} = j, w_\tau = 0, \tau \neq t\}, \alpha, \beta) d\bar{\pi}_j \\
 \int_{\bar{\pi}_k} p(z_{t+1} = l | w_{t+1}, \bar{\pi}_k) p(\bar{\pi}_k | \{\tau | z_{\tau-1} = k, w_\tau = 0, \tau \neq t+1\}, \alpha, \beta) d\bar{\pi}_k \\
 &= \frac{\alpha \beta_k + n_{jk}^{-t}}{\alpha + n_j^{-t}} \frac{\alpha \beta_l + n_{kl}^{-t}}{\alpha + n_k^{-t}}
 \end{aligned} \tag{30}$$

where the quantity $n_{z_{t-1}z_t}$ is the number of times that the transition from state z_{t-1} to state z_t occurred with $w_t = 0$ in the sequence $z_{1:T}$. Furthermore, $n_{z_{t-1}z_t}^{-t}$ is the number of times the transition from state z_{t-1} to z_t occurred with $w_t = 0$, not including the transitions from z_{t-1} to z_t or from z_t to z_{t+1} . Lastly, n_j is the total number of transitions from state j to any other state.

If z_t is equal to $K+1$, that is, a new state has appeared, we will increase K , draw a probability of self-persistence κ_{K+1} for the new state from the prior, and update β using the stick-breaking method. We will sample b from a beta(1, γ) distribution, and assign $\beta_K = b\beta_{k_{\text{new}}}$, $\beta_{k_{\text{new}}} = (1-b)\beta_{k_{\text{new}}}$, where $\beta_{k_{\text{new}}} = \sum_{i=K+1}^{\infty} \beta_i$.

Step 2: Sample $\{\kappa_{j,1}\}$ for $j = 1, \dots, K+1$, and compute $\{\kappa_{j,t+1}\}$ The posterior distribution of $\kappa_{j,1}$ is obtained by applying the beta-binomial conjugate property. The expression for the posterior distribution is given by:

$$\kappa_{j,1} \sim \text{beta} \left(\rho_1 + \sum_{\tau, z_{\tau-1}=j} w_\tau, \rho_2 + \sum_{\tau, z_{\tau-1}=j} 1 - w_\tau \right), j = 1, \dots, K+1 \tag{31}$$

Here, κ_{K+1} represents the self-persistence probability of a new state.

For $t+1$ $\{\kappa_{j,t+1}\}$ can be computed:

$$\begin{aligned}
 \kappa_{j,t+1} &= \frac{e^{v_{j,t}}}{1 + e^{v_{j,t}}} \\
 v_{j,t} &= R_j^T x_t + r_j
 \end{aligned} \tag{32}$$

Step 3: Sequentially sample the auxiliary variables $\{\eta_{j,t}\}$ for $t = 1, \dots, T-1, j = 1, \dots, L$. 7. The conditional posteriors of the Pólya-Gamma random variables are also Pólya-Gamma: $\eta_{j,t} | z_t, (R_j, r_j), x_{t-1} \sim \text{PG}(1, \nu_{j,t})$.

We used samplers implemented in <https://github.com/zoj613/polygamma>.

Step 4: Sample β We introduce auxiliary variables m_{jk} to sample the global transition distribution β . This is done using the Chinese restaurant franchise (CRF) formulation of HDP prior Teh (2006). These variables can be thought of as the number of tables in restaurant j serving dishes k . We first update m_{jk} and then sample β .

For each $(j, k) \in \{1, \dots, K\}^2$, set m_{jk} and s to zero. Then, for $i = 1, \dots, n_{jk}$, draw a sample from a Bernoulli distribution with probability $\frac{\alpha\beta_k}{n+\alpha\beta_k}$. Increase s and if the sample is equal to one, increment m_{jk} . We can then sample β as

$$(\beta_1, \beta_2, \dots, \beta_K, \beta_{k_{\text{new}}}) \sim \text{Dir}(m_{\cdot 1}, \dots, m_{\cdot K}, \gamma), \quad (33)$$

where $\beta_{k_{\text{new}}} = \sum_{i=K+1}^{\infty} \beta_i$ is for transitioning to a new state, and $m_{\cdot k}$ is $\sum_{j=1}^K m_{jk}$. A more thorough explanation of the sampling of β can be found in Fox et al. (2011); Zhou et al. (2021).

Step 5: Sample Hyperparameters $\alpha, \gamma, \rho_1, \rho_2, R, r$ We use the same values of α and γ as in Teh (2006); Escobar and West (1995). By introducing some extra variables, we can make the posterior of α and γ follow a gamma distribution if we assign a gamma prior to them. To handle ρ_1, ρ_2 , we use the reparametrization technique discussed in Chapter 5 of ?. This involves transforming $\phi = \frac{\rho_1}{\rho_1 + \rho_2}, \eta = (\rho_1 + \rho_2)^{-1/3}$, and assigning a Uniform $([0, 1] \times [0, 2])$ prior on (ϕ, η) . Then, we can discretize the support of (ϕ, η) and calculate the posterior numerically.

Let $\eta_{j,t}$ be the auxiliary Pólya-gamma random variable introduced at time t . We can sample values of R_j, r_j from the following posterior:

$$p((R_j, r_j) \mid x_{1:T}, z_{1:T}, \eta_{j,1:T}) \propto p((R_j, r_j)) \prod_{t=1}^T \mathcal{N}(v_{j,t} \mid \lambda_{j,t}/\eta_{j,t}, 1/\eta_{j,t})^{1(z_t=j)}, \quad (34)$$

where $\lambda_{j,t} = w_{t+1} - \frac{1}{2}$.

B Weak limit-sampler

Step 1: Sample $\{z_t, w_t\}_{t=1}^T$ The combined conditional distribution of $z_{1:T}, w_{1:T}$ is determined by

$$\begin{aligned} p(z_{1:T}, w_{1:T} \mid y_{1:T}, \bar{\pi}, \{\kappa_j\}_{j=1}^L, \theta) &= p(z_T, w_T \mid z_{T-1}, y_{1:T}, \bar{\pi}, \{\kappa_j\}_{j=1}^L, \theta) \\ & p(z_{T-1}, w_{T-1} \mid z_{T-2}, y_{1:T}, \bar{\pi}, \{\kappa_j\}_{j=1}^L, \theta) \\ & \cdots p(z_1 \mid y_{1:T}, \bar{\pi}, \{\kappa_j\}_{j=1}^L, \theta). \end{aligned} \quad (35)$$

The conditional probability distribution of z_1 is given by:

$$p(z_1 \mid y_{1:T}, \bar{\pi}, \{\kappa_j\}_{j=1}^L, \theta) \propto p(z_1) p(y_1 \mid \theta_{z_1}) p(y_{2:T} \mid z_1, \bar{\pi}, \{\kappa_j\}_{j=1}^L, \theta) \quad (36)$$

The conditional distribution of $z_t, t > 1$ is given by:

$$\begin{aligned} & p(z_t, w_t \mid z_{t-1}, y_{1:T}, \bar{\pi}, \{\kappa_j\}_{j=1}^L, \theta) \\ & \propto p(z_t, w_t, y_{1:T} \mid z_{t-1}, \bar{\pi}, \{\kappa_j\}_{j=1}^L, \theta) \\ & = p(z_t \mid \bar{\pi}_{z_{t-1}}, w_t) p(w_t \mid z_{t-1}, \{\kappa_j\}_{j=1}^L) p(y_{t:T} \mid z_t, \bar{\pi}, \{\kappa_j\}_{j=1}^L, \theta) p(y_{1:t-1} \mid z_{t-1}, \bar{\pi}, \{\kappa_j\}_{j=1}^L, \theta) \\ & \propto p(z_t \mid \bar{\pi}_{z_{t-1}}, w_t) p(w_t \mid z_{t-1}, \{\kappa_j\}_{j=1}^L) p(y_{t:T} \mid z_t, \bar{\pi}, \{\kappa_j\}_{j=1}^L, \theta) \\ & = p(z_t \mid \bar{\pi}_{z_{t-1}}, w_t) p(w_t \mid z_{t-1}, \{\kappa_j\}_{j=1}^L) p(y_t \mid \theta_{z_t}) m_{t+1,t}(z_t), \end{aligned} \quad (37)$$

The backward message passed from z_t to z_{t-1} , denoted by $m_{t+1,t}(z_t)$, is the probability of observing $y_{t+1:T}$ given

z_t , $\bar{\pi}$, $\{\kappa_{j,t}\}_{j=1}^L$, and θ . This is recursively defined as follows:

$$m_{t+1,t}(z_t) = \sum_{z_{t+1}, w_{t+1}} p(z_{t+1} | \bar{\pi}_{z_t}, w_{t+1}) p(w_{t+1} | z_t, \{\kappa_{j,t+1}\}_{j=1}^L) p(y_{t+1} | \theta_{z_{t+1}}) m_{t+2,t+1}(z_{t+1}), t \leq T$$

$$m_{T+1,T}(z_T) = 1$$
(38)

Step 2: Sample $\{\kappa_{j,1}\}$ for $j = 1, \dots, K+1$, and compute $\{\kappa_{j,t+1}\}$ Same as in direct assignment sampler step 2, but for $j = 1, \dots, L$.

Step 3: Sample $\{\beta_j\}_{j=1}^L, \{\bar{\pi}_j\}_{j=1}^L$

$$\beta | m, \gamma \sim \text{Dir}(\gamma/L + m_{\cdot 1}, \dots, \gamma/L + m_{\cdot L}),$$

$$\bar{\pi}_j | z_{1:T}, w_{1:T}, \alpha, \beta \sim \text{Dir}(\alpha\beta_1 + n_{j1}, \dots, \alpha\beta_L + n_{jL}), j = 1, \dots, L.$$
(39)

Step 4: Sample $\{\theta_j\}_{j=1}^L$ We draw θ from the posterior distribution based on the emission function and the base measure H of the parameter space Θ , i.e. $\theta_j | z_{1:T}, y_{1:T} \sim p(\theta_j | \{y_t | z_t = j\})$. For all the emissions in the main paper, we can conveniently sample θ_j from its posterior due to the conjugacy properties.

Step 5: Sample Hyperparameters $\alpha, \gamma, \rho_1, \rho_2$ Same as step 4 in direct assignment sampler.

C MNIW Prior

In the autoregressive emission, the MNIW prior is established by assigning a matrix-normal prior $\mathcal{MN}(M, \Sigma_j, V)$ to A_j conditioned on Σ_j :

$$p(A_j | \Sigma_j) = \frac{1}{(2\pi)^{d^2/2} |V|^{d/2} |\Sigma_j|^{d/2}} \exp\left(-\frac{1}{2} \text{tr}\left[(A_j - M)^\top \Sigma_j^{-1} (A_j - M) V^{-1}\right]\right),$$
(40)

where M is $d \times d$ matrix, Σ_j, V are $d \times d$ positive-definite matrix, d is the dimension of observation y_t ; and an inverse-Wishart prior $IW(S_0, n_0)$ on Σ_j :

$$p(\Sigma_j) = \frac{|S_0|^{n_0/2}}{2^{n_0 d/2} \Gamma_d(n_0/2)} |\Sigma_j|^{-(n_0+d+1)/2} \exp\left(-\frac{1}{2} \text{tr}(\Sigma_j^{-1} S_0)\right),$$
(41)

where $\Gamma_d(\cdot)$ denotes the multivariate gamma function. We define $M = \mathbf{0}$, $V = I_{d \times d}$, $n_0 = d + 2$, and $S_0 = 0.4\bar{\Sigma}$, with $\bar{\Sigma}$ being $\frac{1}{T} \sum_{t=1}^{T-1} (x_t - \bar{x})(x_t - \bar{x})^\top$, and $x_t = y_{t+1} - y_t$.